Heat capacity and magnetic phase diagram of the low-dimensional antiferromagnet Y_2BaCuO_5

2008 J. Phys.: Condens. Matter 20 335208

(http://iopscience.iop.org/0953-8984/20/33/335208)

J. Phys.: Condens. Matter **20** (2008) 335208 (7pp) doi:10.1088/0953-8984/20/33/335208

Heat capacity and magnetic phase diagram of the low-dimensional antiferromagnet Y_2BaCuO_5

W Knafo[1,2,3], C Meingast[1], A Inaba[4], Th Wolf[1] and H v Löhneysen[1,2]

[1] Forschungszentrum Karlsruhe, Institut für Festkörperphysik, D-76021 Karlsruhe, Germany
[2] Physikalisches Institut, Universität Karlsruhe, D-76128 Karlsruhe, Germany
[3] Laboratoire National des Champs Magnétiques Pulsés, UMR CNRS-UPS-INSA 5147, 143 avenue de Rangueil, 31400 Toulouse, France
[4] Research Center for Molecular Thermodynamics, Graduate School of Science, Osaka University, Toyonaka, Osaka 560-0043, Japan

Received 28 January 2008, in final form 30 May 2008
Published 22 July 2008
Online at stacks.iop.org/JPhysCM/20/335208

Abstract

A study by specific heat of a polycrystalline sample of the low-dimensional magnetic system Y_2BaCuO_5 is presented. Magnetic fields up to 14 T are applied and permit us to extract the (T, H) phase diagram. Below $\mu_0 H^* \simeq 2$ T, the Néel temperature, associated with a three-dimensional antiferromagnetic long-range ordering, is constant and equals $T_N = 15.6$ K. Above H^*, T_N increases linearly with H and a field-induced increase of the entropy at T_N is related to the presence of an isosbestic point at $T_X \simeq 20$ K, where all the specific-heat curves cross. A comparison is made between Y_2BaCuO_5 and the quasi-two-dimensional magnetic systems $BaNi_2V_2O_8$, $Sr_2CuO_2Cl_2$ and Pr_2CuO_4, for which very similar phase diagrams have been reported. An effective field-induced magnetic anisotropy is proposed to explain these phase diagrams.

(Some figures in this article are in colour only in the electronic version)

1. Introduction

Because of their layered structure, the undoped high-temperature superconducting cuprates are low-dimensional magnetic systems. Indeed, Cu–O–Cu superexchange paths within the planes are responsible for a strong two-dimensional (2D) magnetic exchange $J \simeq 1000$ K between the $S = 1/2$ spins of the Cu^{2+} ions. In the undoped state, three-dimensional (3D) long-range ordering occurs below a Néel temperature T_N of about several hundred Kelvin [1, 2], due to a small additional magnetic exchange J' between the layers. At the magnetic quantum phase transition of some heavy-fermion systems, the appearance of superconductivity is believed to arise from an enhancement of the magnetic fluctuations [3, 4]. Hence, a better understanding of the magnetic properties of the high-T_C cuprates could be of primary importance to elucidate why superconductivity develops in these systems [5]. However, the magnetic energy scales are rather high (several hundred Kelvin) and their investigation is difficult to perform, due to the loss of oxygen and to the sample melting at high temperatures.

A possible alternative is to study the magnetic properties of systems similar to the high-T_C cuprates, but with much smaller magnetic energy scales. One of them is the 'green phase' compound Y_2BaCuO_5, which is known as an impurity phase of the high-T_C $YBa_2Cu_3O_{6+\delta}$ [6] and whose green color indicates its insulating character. As in the high-T_C cuprates, the magnetic properties of Y_2BaCuO_5 are strongly low-dimensional and originate from the $S = 1/2$ Cu^{2+} ions. Indeed, broad anomalies in the magnetic susceptibility and in the specific heat, whose maxima were reported at $T_{max} \simeq 30$ K [7] and $T'_{max} \simeq 20$ K [8], respectively, are believed to be due to the low-dimensional magnetic exchange of Y_2BaCuO_5. However, and contrary to the layered high T_C cuprates where the magnetic exchange is quasi-2D, Y_2BaCuO_5 has a rather complex 3D lattice structure, shown in figure 1, and the question whether the dominant magnetic interactions are one-dimensional (1D) or 2D is still open. Three kinds of Cu–O–O–Cu superexchange paths, either 1D or 2D, were suggested [9]. It is unclear, however, which one of the three paths is dominating. The fact that, in Y_2BaCuO_5, the

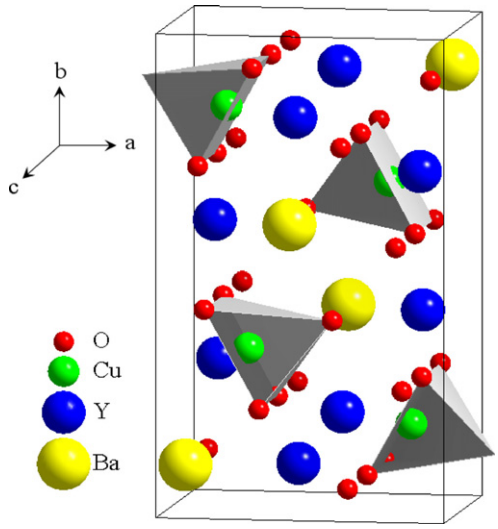

Figure 1. Lattice unit cell of Y_2BaCuO_5, where the CuO_5 pyramids are represented in gray.

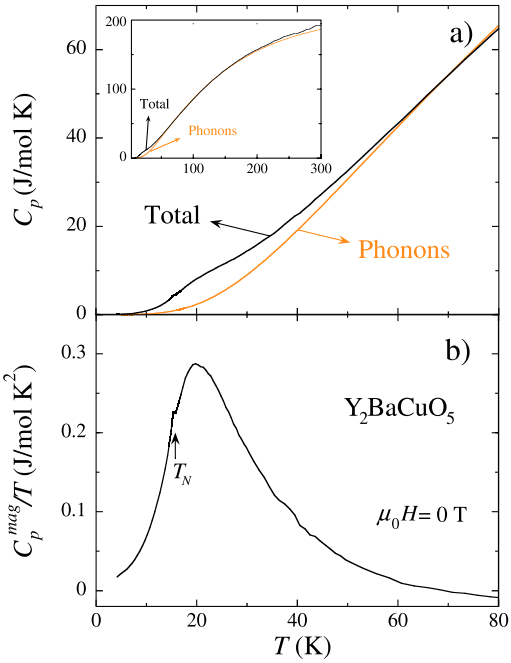

Figure 2. (a) Total and lattice specific heat of Y_2BaCuO_5 in a C_p versus T plot, with T up to 80 K; data are plotted up to 300 K in the inset. (b) Magnetic specific heat C_p^{mag} of Y_2BaCuO_5, in a C_p^{mag}/T versus T plot. Above 60 K, C_p^{mag} is less than 2% of the total specific heat C_p.

superexchange paths go through two oxygens, in contrast to one oxygen for $YBa_2Cu_3O_{6+\delta}$, explains the smaller magnetic energy scales [9]. At lower temperatures, 3D antiferromagnetic long-range ordering sets in below the Néel temperature $T_N \simeq 15.5$ K [9, 10], induced by the combination of the strong low-dimensional and additional tiny 3D magnetic interactions, but also of spin anisotropy, as we will show here.

In this paper, we present a study of the specific heat of Y_2BaCuO_5 under magnetic fields up to 14 T, which permits us to extract the (T, H) phase diagram of this system. In the discussion, we compare the phase diagram of Y_2BaCuO_5 to similar phase diagrams obtained for other low-dimensional systems, and we propose to explain them using the picture of an effective field-induced anisotropy.

2. Experimental details

The polycrystalline sample of Y_2BaCuO_5 studied here was synthesized by the direct method in air. Appropriate amounts of Y_2O_3, $BaCO_3$ and CuO were mixed intensely, then pressed into pellets and finally reaction sintered with increasing temperature steps between 750 and 960 °C, without intermediate grinding. X-ray powder diffractometry did not show any trace of impurity phases. Except for 730 ppm Sr and 222 ppm Fe, no other impurities were detected by x-ray fluorescence analysis. The specific heat was measured under magnetic fields up to 14 T using a physical properties measurement system (PPMS) from Quantum Design, and using an adiabatic calorimeter at zero field up to 400 K [11]. The specific heats below 200 K obtained by both methods agree well with each other. To enhance the resolution in the vicinity of the magnetic phase transitions, the relaxation curves from the PPMS were analyzed following a procedure similar to the one proposed by Lashley *et al* [12]. Here we will show only the PPMS data.

3. Results

Figure 2(a) shows the total specific heat $C_p(T)$ of Y_2BaCuO_5 measured at zero magnetic field, together with the phonon background $C_p^{ph}(T)$. $C_p^{ph}(T)$ was estimated using an appropriate scaling of the non-magnetic specific heat of $YBa_2Cu_3O_7$.[5] Figure 2(a) shows $C_p(T)$ and $C_p^{ph}(T)$ for temperatures up to 80 K, while the Inset shows the data for temperatures up to 300 K. These plots indicate that the specific heat of Y_2BaCuO_5 is almost purely phononic above 70 K and that a magnetic signal develops below roughly 70 K. In figure 2(b), the magnetic contribution to the specific heat, calculated using $C_p^{mag}(T) = C_p(T) - C_p^{ph}(T)$, is shown in a $C_p^{mag}(T)/T$ versus T plot. C_p^{mag} is characterized by a broad anomaly, whose maximum occurs at about 20 K, and by a small jump at $T_N \simeq 15$ K, as typically observed for low-dimensional systems [14, 15]. The integration of $C_p^{mag}(T)/T$ up to 70 K leads to an entropy change of $\Delta S_{mag} \simeq 6.7$ J mol^{-1} K^{-1}, which equals, within 15%, the total entropy $R \ln 2 \simeq 5.76$ J mol^{-1} K^{-1} expected for the $S = 1/2$ spins and shows that our estimation of the phonon background is reasonable [13] (also see footnote 5). Figure 3 focuses on the tiny specific-heat anomaly at the 3D long-range antiferromagnetic ordering transition T_N, which was

[5] The phonon contribution to the specific heat of $YBa_2Cu_3O_7$, denoted $C_p^{ph,123}(T)$, was calculated by Bohnen and Heid from the density of states determined within density functional theory [13]. Knowing that there are 9 and 13 atoms per Y_2BaCuO_5 and $YBa_2Cu_3O_7$ formulae, respectively, we estimated the phonon background of Y_2BaCuO_5 by $C_p^{ph}(T) = 9/13 * C_p^{ph,123}(1.08 * T)$. The factor 1.08 was adjusted so that $C_p(T) \simeq C_p^{ph}(T)$ above 100 K, where the signal is assumed to be only of phononic origin.

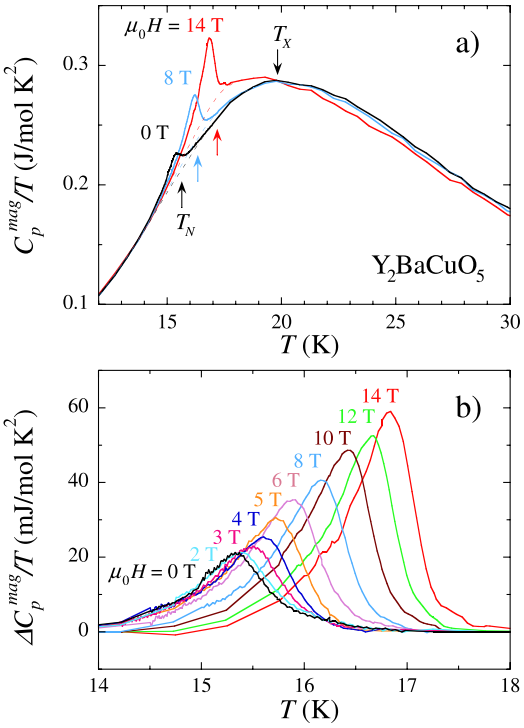

Figure 3. (a) Magnetic specific heat $C_p^{\rm mag}$ of Y_2BaCuO_5 in a $C_p^{\rm mag}/T$ versus T plot, at $\mu_0H = 0$, 8 and 14 T. The dotted lines indicate the background used to separate the anomaly at $T_{\rm N}$. (b) Anomaly $\Delta C_p^{\rm mag}$ of Y_2BaCuO_5 at $T_{\rm N}$, in a $\Delta C_p^{\rm mag}/T$ versus T plot, for magnetic fields $0 \leqslant \mu_0H \leqslant 14$ T.

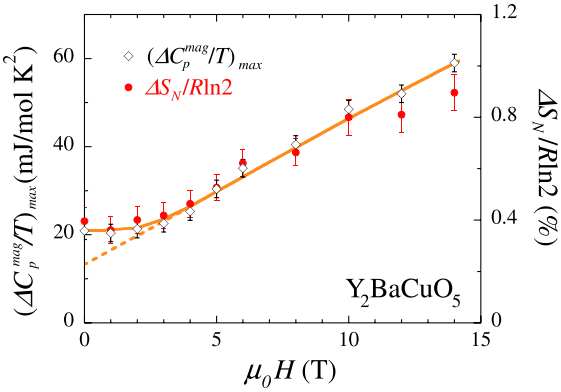

Figure 4. Variation with H of the jump $(\Delta C_p^{\rm mag}/T)_{\rm max}$ in the specific heat at the Néel ordering and of the associated entropy change $\Delta S_{\rm N}$.

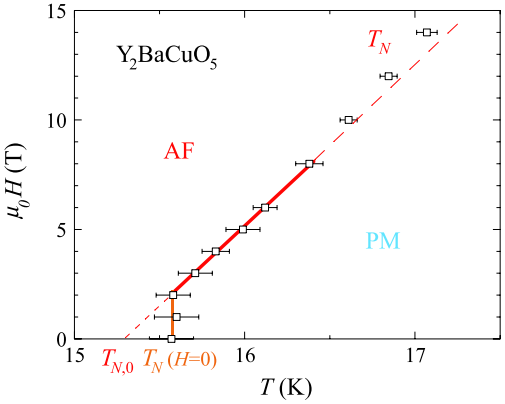

Figure 5. (T, H) phase diagram of Y_2BaCuO_5 (polycrystal) obtained by specific-heat measurements (AF = antiferromagnetic phase, PM = high-temperature paramagnetic regime).

first reported by Gros *et al* [10]. In the following, we will concentrate on the effects of the magnetic field on this anomaly.

In figure 3(a), the magnetic specific heat of Y_2BaCuO_5 is shown for the magnetic fields $\mu_0H = 0$, 8 and 14 T in a $C_p^{\rm mag}(T)/T$ versus T plot. The Néel temperature $T_{\rm N}$ and the size of the anomaly at the antiferromagnetic transition both increase with increasing H. Above $T_{\rm N}$, all the curves cross at an isosbestic point [16] at $T_X \simeq 20$ K, which will be discussed in section 4. For each magnetic field, an appropriate background (dotted lines in figure 3(a)) is used to obtain the anomaly $\Delta C_p^{\rm mag}(T)$ associated with the 3D magnetic ordering. In figure 3(b), a plot of $\Delta C_p^{\rm mag}(T)/T$ obtained for various fields up to 14 T emphasizes the field-induced increases of $T_{\rm N}$ and of the size of the anomaly at the antiferromagnetic transition. Its typical width, of about 0.8 K (full width at half-maximum), is almost unaffected by the magnetic field and could arise from sample imperfections (strains, impurities, etc) or from the polycrystalline nature of the sample.

In figure 4, the jump $(\Delta C_p^{\rm mag}/T)_{\rm max}$ in the specific heat at $T_{\rm N}$ and the associated entropy change $\Delta S_{\rm N}$ are[6] plotted as a function of H. Since the width of the anomaly is almost unaffected by H, similar field dependences are obtained for $(\Delta C_p^{\rm mag}/T)_{\rm max}$ and $\Delta S_{\rm N}$: both are nearly constant for $\mu_0H \leqslant \mu_0H^* \approx 2$ T and then increase roughly linearly with H for $H \geqslant H^*$. The small value $\Delta S_{\rm N}(H = 0)/\Delta S_{\rm mag} = (4.0 \pm 0.5) \times 10^{-3}$ is a consequence of the low-dimensional character of the magnetic exchange [14], $\Delta S_{\rm N}$ being enhanced by a factor of 2.5 at $\mu_0H = 14$ T.

In figure 5, the T–H phase diagram of Y_2BaCuO_5 is shown for magnetic fields up to 14 T, $T_{\rm N}$ being defined at the minimum of the slope of $\Delta C_p^{\rm mag}/T$.[7] The Néel temperature $T_{\rm N}$ is independent of H for $\mu_0H \leqslant \mu_0H^* \simeq 2$ T, with $T_{\rm N}(H = 0) = 15.6 \pm 0.1$ K, and increases linearly with H for $H \geqslant H^*$, where $T_{\rm N}(H) = T_{\rm N,0} + aH$, with $T_{\rm N,0} = 15.3 \pm 0.1$ K and $a = 0.14 \pm 0.02$ K T^{-1} (above 10 T a slight deviation from this regime is observed). In section 4, the field-induced increases of $T_{\rm N}$ and $\Delta S_{\rm N}$ will be qualitatively explained using the picture of a field-induced anisotropy.

4. Discussion

4.1. Phase diagram of Y_2BaCuO_5—explanation in terms of field-induced anisotropy

The phase diagram of the low-dimensional magnetic system Y_2BaCuO_5 (figure 5) is very similar to those of the quasi-2D magnetic systems $BaNi_2V_2O_8$ [15], $Sr_2CuO_2Cl_2$ [17] and Pr_2CuO_4 [18] (see section 4.2) and we interpret them

[6] For each magnetic field, $(\Delta C_p^{\rm mag}/T)_{\rm max}$ corresponds to the maximal value of $\Delta C_p^{\rm mag}(T)/T$ and $\Delta S_{\rm N}$ is obtained by integration of $\Delta C_p^{\rm mag}(T)$ (figure 3(b)).

[7] The shape of the antiferromagnetic anomaly (figure 3 (b)) is characteristic of a second-order phase transition broadened by some sample inhomogeneities. While a pure, thus nonbroadened, second-order transition leads to a step-like anomaly at $T_{\rm N}$ in the specific heat, the present case consists in a broad transition where $T_{\rm N}$ can be defined at the minimum of the slope of $C_p(T)$.

similarly, using a picture introduced 30 years ago by Villain and Loveluck for quasi-1D antiferromagnetic systems [19]. In this picture, the increase of $T_N(H)$ is induced by a reduction of the spin fluctuations parallel to **H**, due to an alignment of the antiferromagnetic fluctuations, as well as the antiferromagnetically coupled static spins, perpendicular to **H**. This effect can be described by an effective field-induced anisotropy, whose easy axis is $\perp$ **H** [20] and which competes with the intrinsic anisotropy of the system. As long as the field-induced anisotropy is weaker than the intrinsic anisotropy, i.e. for $H \leqslant H^*$, $T_N(H)$ is unaffected by the magnetic field and the spins align along the intrinsic easy axes. For $H \geqslant H^*$, the field-induced anisotropy is stronger than the intrinsic anisotropy and $T_N(H)$ is controlled by H, the spins being aligned along the field-induced easy axes ($\perp$ **H**).

The crossing point of the specific-heat data of Y_2BaCuO_5 at $T_X \simeq 20$ K (figure 3(a)) is, to the best of our knowledge, the first isosbestic point [16] reported in the thermodynamic properties of a low-dimensional magnetic system. This effect is the consequence of a transfer of the specific-heat weight, with respect to the conservation of the magnetic entropy ΔS_{mag}. Indeed, our data show that the application of a magnetic field leads to a gain of entropy at T_N, i.e. below T_X, which equals approximately the loss of entropy above T_X. Consistent with the picture introduced above, we propose that the isosbestic point at T_X is due to a field-induced transfer of the specific-heat weight from the large and broad low-dimensional short-range ordering anomaly to the small 3D long-range ordering anomaly at T_N.

Little is known microscopically about the magnetic properties of Y_2BaCuO_5, i.e. about the exact nature of the exchange interactions and of the magnetic anisotropy. The non-layered crystal structure of Y_2BaCuO_5 (see figure 1) precludes a prediction of the superexchange paths, the dominant paths being probably 1D or 2D [9]. The shapes of the magnetic susceptibility [7] and of the specific heat [8] just indicate that the dominant exchange interactions have a low-dimensional character, either 1D or 2D [9]. Some authors suggested a 2D character of the exchange and an XY anisotropy, from appropriate fits of the magnetic susceptibility [7, 21] and of the ESR linewidth [22], respectively, but these results cannot be considered as definitive proofs. The nature of the antiferromagnetic ordering below T_N is also unclear, since several structures have been proposed, where the spins are aligned either in the (**a**, **c**) plane [9, 23] or along **c** [24] (cf. [22] for a summary of the proposed magnetic structures). Further experimental studies on single crystals, such as by magnetization and neutron scattering techniques, are necessary to determine unambiguously the nature of the spin anisotropy and of the magnetic exchange in Y_2BaCuO_5, which cannot be predicted from the complex three-dimensional structure of Y_2BaCuO_5 (figure 1). However, we interpret the high-field increase of $T_N(H)$ in Y_2BaCuO_5 as a consequence of a field-induced anisotropy, a picture that works for both quasi-1D systems [19] and quasi-2D systems [15], the intrinsic spin anisotropy being always ultimately of Ising kind. A knowledge of the nature of the intrinsic anisotropy and of the magnetic exchange would be necessary for a more quantitative understanding of the properties of Y_2BaCuO_5.

An additional difficulty arises from the fact that the results presented here were obtained on a polycrystalline sample of Y_2BaCuO_5, so that our phase diagram is equivalent to take the average of the phase diagrams of a single crystal over all possible field directions. In the quasi-2D magnet $BaNi_2V_2O_8$, there is hardly any modification of the magnetic properties when **H** $\parallel$ **c** (hard axis) [25], which implies that a phase diagram obtained with a polycrystalline sample would be similar to the phase diagram reported for **H** $\perp$ **c** [15], possibly with a slight broadening of the transition. By analogy, we believe that it is reasonable to interpret the phase diagram of a polycrystalline Y_2BaCuO_5 similarly to the phase diagram that would be obtained for a single crystal with **H** parallel to the easy axis or to the easy plane (depending on the nature of the anisotropy).

The extrapolation of the 'high-field' linear behavior of $T_N(H)$ to zero field leads to a temperature $T_{N,0}$ smaller than $T_N(H = 0)$ by $\Delta = 0.3$ K. As proposed for $BaNi_2V_2O_8$, $Sr_2CuO_2Cl_2$ and Pr_2CuO_4 [15] (see also section 4.2), we speculate that, in Y_2BaCuO_5, $T_{N,0}$ is a virtual ordering temperature, which would characterize the system in the limit of no easy-axis anisotropy. In this picture, the increase of $T_N(H = 0)$ by Δ is a consequence of the intrinsic easy-axis anisotropy. A linear extrapolation of the high-field variation of $\Delta S_N(H)$ also leads to $\Delta S_{N,0}/\Delta S_{mag} = (2.3 \pm 0.5) \times 10^{-3}$ at $H = 0$ (cf. figure 4). As well as $T_{N,0}$, we associate the extrapolated entropy change $\Delta S_{N,0}/\Delta S_{mag}$ with the limit of no easy-axis anisotropy. At zero magnetic field, the Néel temperature $T_N(H = 0)$ and the associated change of entropy $\Delta S_N(H = 0)$ have non-zero values, probably because of the combination of the magnetic anisotropy (XY and Ising) and of a 3D character of the magnetic exchange[8].

4.2. Similarities between the phase diagram of Y_2BaCuO_5 and those of the quasi-2D $BaNi_2V_2O_8$, $Sr_2CuO_2Cl_2$ and Pr_2CuO_4

As mentioned above, the T–H phase diagram of polycrystalline Y_2BaCuO_5, shown in figure 5, has a striking resemblance with the phase diagrams of single crystals of the quasi-2D antiferromagnets $BaNi_2V_2O_8$ [15], $Sr_2CuO_2Cl_2$ [17] and Pr_2CuO_4 [18], which are shown in figures 6(a)–(c), respectively, for H applied within the easy plane[9]. In these insulating systems, $T_N(H)$ is constant for $H \leqslant H^*$ and increases with H for $H \geqslant H^*$. A linear increase of $T_N(H)$ is unambiguously obtained in the high-field regime of Y_2BaCuO_5 and $BaNi_2V_2O_8$ [15] and is compatible, within the experimental errors, with the phase diagrams of $Sr_2CuO_2Cl_2$ [17] and

[8] Only 3D systems and 2D Ising systems exhibit long-range magnetic ordering at a non-zero temperature (De Jongh [26]). If a magnetic system is purely 1D, or purely 2D Heisenberg or XY, no long-range ordering can be attained at non-zero temperature. Pure 2D XY systems correspond to a particular case, where a topological short-range ordering can theoretically occur at a Berezinskii–Kosterlitz–Thouless temperature $T_{BKT} > 0$ (Berezinskii and Kosterlitz [26]). A magnetic entropy associated to a transition can thus be only obtained if the system is 3D Ising, 3D XY, 3D Heisenberg, 2D Ising or 2D XY.

[9] While the phase diagram of Y_2BaCuO_5 was obtained here from the specific heat, those of $BaNi_2V_2O_8$, $Sr_2CuO_2Cl_2$ and Pr_2CuO_4 were obtained from specific heat and thermal expansion [15], magnetization and NMR [17], and neutron scattering [18], respectively.

Table 1. Characteristics of the magnetic properties of Y_2BaCuO_5, $BaNi_2V_2O_8$, $Sr_2CuO_2Cl_2$ and Pr_2CuO_4.

	Y_2BaCuO_5	$BaNi_2V_2O_8$	$Sr_2CuO_2Cl_2$	Pr_2CuO_4
T_{max} (K)[a,b]	30	150	n.d.	n.d.
$T_N(H=0)$ (K)	15.6	47.4	256.5	282.8
$\Delta S_N(H=0)/\Delta S_{mag}$	4×10^{-3}	7×10^{-4}	n.d.	n.d.
H [c]	(polycrystal)	$\perp$ **c**	$\perp$ **c**	$\perp$ **c**
$\mu_0 H^*$ (T)[a,c]	$\simeq$2	$\simeq$1.5	$\simeq$1.5	$\simeq$2
$T_{N,0}$ (K)[c]	15.3	46.6	254	282.4
a(K T^{-1})[c]	0.14	0.34	2	0.3
$\Delta S_{N,0}/\Delta S_{mag}$ [c]	2.3×10^{-3}	n.d.	n.d.	n.d.
Symmetry	orth.	hex.	tetr.	tetr.
Ref.	[7]	[15, 27]	[17]	[18]

[a] Defined as the temperature of the maximum of $\chi(T)$.
[b] n.d. = nondetermined, hex. = hexagonal, orth. = orthorhombic, tetr. = tetragonal.
[c] $T_N(H) = T_{N,0} + aH$ and $\Delta S_N(H) \simeq \Delta S_{N,0} + bH$ for $H \geqslant H^*$.

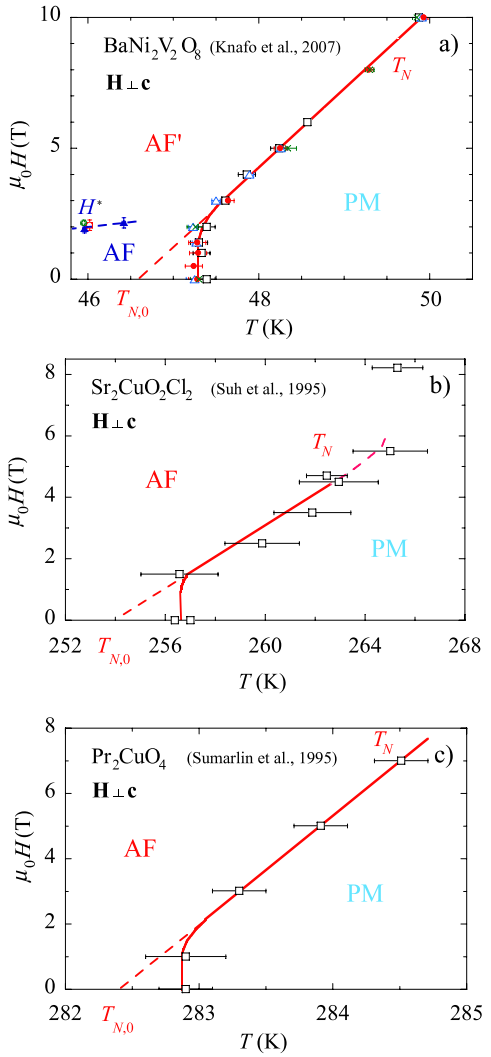

Figure 6. (T, H) phase diagrams of the quasi-2D magnetic systems (a) $BaNi_2V_2O_8$ [15], (b) $Sr_2CuO_2Cl_2$ [17] and (c) Pr_2CuO_4 [18], with **H** $\perp$ **c**. The data in (b) and (c) were scanned from [17] and [18].

Pr_2CuO_4 [18]. In table 1, $T_N(H=0)$, $T_{N,0}$, H^* and a (from a fit by $T_N(H) = T_{N,0} + aH$ for $H > H^*$) are given for each of these systems. For Y_2BaCuO_5 [7] and $BaNi_2V_2O_8$ [27], the temperature T_{max} of the maximum of the magnetic susceptibility $\chi(T)$, characteristic of the low-dimensional magnetic exchange, is also given. The investigation of the magnetic properties of these two systems is rather easy, since their full magnetic entropy is contained below room temperature (see section 3 and [15]), as illustrated by the rather small values of T_N and T_{max}, which are of the order of several tens of Kelvin. In contrast, the magnetic properties of $Sr_2CuO_2Cl_2$ and Pr_2CuO_4, as well as those of the underdoped high-T_C cuprates, are more difficult to investigate, being associated with temperature scales $T_{max} > T_N \simeq 300$ K.[10]

We interpret the enhancement of $T_N(H)$ with increasing magnetic field in $BaNi_2V_2O_8$, $Sr_2CuO_2Cl_2$ and Pr_2CuO_4, as well as the one observed in Y_2BaCuO_5, using an effective field-induced anisotropy [19]. Contrary to the present work, which was made using a polycrystal of Y_2BaCuO_5, the studies of $BaNi_2V_2O_8$, $Sr_2CuO_2Cl_2$ and Pr_2CuO_4 were performed on single crystals with **H** $\perp$ **c** [15, 17, 18]. While the magnetic properties of Y_2BaCuO_5 cannot be easily related to its 3D and rather complex crystal structure (figure 1), the quasi-2D magnetic exchange paths of $BaNi_2V_2O_8$, $Sr_2CuO_2Cl_2$ and Pr_2CuO_4 are a direct consequence of their layered crystallographic structure, and their intrinsic anisotropy is controlled by the symmetry of their lattice. The intrinsic in-plane anisotropy, hexagonal for $BaNi_2V_2O_8$ [27] and tetragonal for $Sr_2CuO_2Cl_2$ [17] and Pr_2CuO_4 [18], leads to magnetic domains at zero field where the spins align (in the easy plane) along one of three equivalent easy axes in $BaNi_2V_2O_8$ and along one of two equivalent easy axes in $Sr_2CuO_2Cl_2$ and Pr_2CuO_4 [17, 18, 27]. In [17], Suh *et al* proposed that the change of behavior of $T_N(H)$, which occurs at $\mu_0 H^* \simeq 2$ T in $Sr_2CuO_2Cl_2$, is related to a field-induced crossover from a regime controlled by the intrinsic XY anisotropy to a regime controlled by the field-induced Ising anisotropy. For $Sr_2CuO_2Cl_2$, but also for $BaNi_2V_2O_8$ and Pr_2CuO_4, we propose that the change of behavior of $T_N(H)$ at H^* results in fact from a crossover between a regime controlled by the intrinsic Ising-like in-plane anisotropy (with two or

[10] To the best of our knowledge, the magnetic susceptibility of these systems has never been measured above room temperature. We note that, for the quasi-2D La_2CuO_4, which belongs to the same family as $Sr_2CuO_2Cl_2$ and Pr_2CuO_4, a maximum of $\chi(T)$ occurs at about 1000 K and antiferromagnetic ordering is established below $T_N \simeq 300$ K [28].

three equivalent easy axes) to a regime controlled by the field-induced Ising anisotropy (with one easy axis) [15]. Although the XY anisotropy plays an important role in both regimes above and below H^*, we believe that the crossover at H^* is not directly related to the XY anisotropy, as proposed in [17], but is due to the small residual Ising-like anisotropy, which ultimately determines the easy axis within the XY plane.

We furthermore speculate that, for $Sr_2CuO_2Cl_2$ and Pr_2CuO_4, as well as for $BaNi_2V_2O_8$ [15], $T_{N,0}$ corresponds to a 'virtual' Néel temperature which would be achieved in a limit with no in-plane anisotropy, being controlled by the combination of the 2D exchange, the XY anisotropy and the interlayer 3D exchange. Thus, $T_{N,0}$ would give an upper limit of the Berezinskii–Kosterlitz–Thouless temperature T_{BKT}, characteristic of a pure 2D XY magnetic system [26]. Moreover, $T_{N,0}$ and T_{BKT} would be equal if the interlayer exchange would be negligible. This would also apply for Y_2BaCuO_5 if one could prove, e.g. by neutron scattering, that it is quasi-2D (thus not quasi-1D). Since a strictly low-dimensional (1D or 2D) Heisenberg system corresponds to a limit with no transition [26], thus with $\Delta S_N \to 0$, the fact that $\Delta S_N(H = 0)/\Delta S_{mag}$ is six times smaller in $BaNi_2V_2O_8$ than in Y_2BaCuO_5 (table 1) indicates a stronger low-dimensional character in $BaNi_2V_2O_8$ than in Y_2BaCuO_5. The non-zero values of $T_{N,0}$ and $\Delta S_{N,0}$ in Y_2BaCuO_5 are the consequence of the XY anisotropy and/or of the 3D exchange, in addition to the low-dimensional exchange (1D or 2D) [26].

In [14] Bloembergen compared the specific-heat data of several quasi-2D magnetic systems. He discussed how the residual 3D intralayer exchange, as well as XY and in-plane anisotropies, stabilize long-range ordering in these systems, leading to an increase of T_N and of the size of the associated specific-heat anomaly. Our data, but also our interpretation, are very similar to the ones of Bloembergen [14] (cf. the heat-capacity data from figure 3 of the present paper and from figures 2 and 3 of [14]). As an important new feature, our work shows that a magnetic field can be used to continuously tune the magnetic anisotropy of low-dimensional systems.

In figure 7, we present a tentative extension to very high magnetic fields of the phase diagrams of Y_2BaCuO_5, $BaNi_2V_2O_8$, $Sr_2CuO_2Cl_2$ and Pr_2CuO_4. In these systems, the low-dimensional (1D or 2D) exchange J is the dominant magnetic energy scale and a ferromagnetic polarized regime, where the spins are aligned parallel to the magnetic field, has to be reached at magnetic fields $H > H_J$, with $H_J \propto J$. This implies that the phase line $T_N(H)$, which first increases linearly, as reported here, will reach a maximum before decreasing down to zero at H_J, the spins being in a canted antiferromagnetic state for $H^* < H < H_J$. As shown by the broad maxima observed in the heat-capacity and magnetic susceptibility measurements, a crossover occurs at zero field at $T_J \propto J$, which corresponds to the onset of low-dimensional short-range ordering and consists of low-dimensional antiferromagnetic fluctuations. The application of a magnetic field is expected to decrease T_J and we speculate that $T_J(H)$ will merge at very high fields with the transition line $T_N(H)$ of the canted ordered state, since $T_N(H)$ will cancel out at $H_J \propto J \propto T_J(H = 0)$. Finally, a crossover

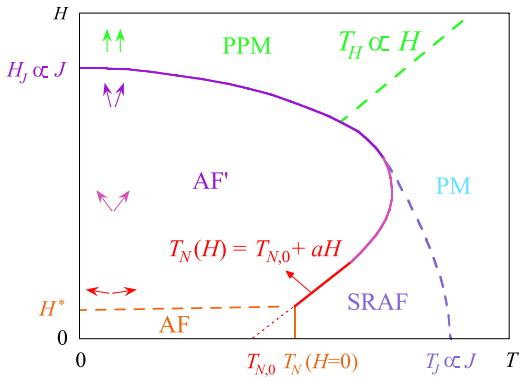

Figure 7. Phase diagram expected at high enough magnetic fields for Y_2BaCuO_5, $BaNi_2V_2O_8$, $Sr_2CuO_2Cl_2$ and Pr_2CuO_4 (AF = low-field antiferromagnetic phase, AF′ = field-induced canted phase, PPM = high-field polarized paramagnetic phase, PM = high-temperature paramagnetic regime, and SRAF = low-dimensional short-range antiferromagnetic regime).

characteristic of the field-induced polarized state is expected to occur at $T_H \propto H$. Pulsed magnetic fields should be used to extend the phase diagram presented in figure 5 up to much higher fields, in order to try to reach its polarized state and to check the validity of the tentative phase diagram of figure 7. This should enable one to extract the different magnetic energy scales and lead to a better understanding of the magnetic properties of Y_2BaCuO_5.

5. Conclusion

The T–H phase diagram of the low-dimensional magnetic system Y_2BaCuO_5 determined by heat-capacity measurements has revealed striking resemblances with the phase diagrams of the quasi-2D magnetic systems $BaNi_2V_2O_8$, $Sr_2CuO_2Cl_2$ and Pr_2CuO_4. Although we do not know the nature of the exchange (quasi-1D or quasi-2D) and of the magnetic anisotropy in Y_2BaCuO_5, we interpret the increase of $T_N(H)$ as resulting from a field-induced anisotropy. In this scenario, at the lowest energy or corresponding field scales, the Ising-like anisotropy is important. Further, our work permitted us to demonstrate that external magnetic fields can be used to continuously tune an effective spin anisotropy. We observed a field-induced transfer of magnetic entropy from the low-dimensional high-temperature broad signal to the anomaly associated with the 3D ordering at T_N, which is related to the presence of an isosbestic point at $T_X \simeq 20$ K.

The comparison of the magnetic properties of Y_2BaCuO_5, $BaNi_2V_2O_8$, $Sr_2CuO_2Cl_2$ and Pr_2CuO_4 should be useful to refine theoretical models. New theoretical developments are needed to understand these properties on a more quantitative level, notably the linear increase of T_N with H at moderate magnetic fields. The theories, which already consider the XY anisotropy and the different kinds of exchange interactions (see, for example, [29]), should be extended to include an Ising-like anisotropy term, which ultimately determines the direction of the ordered spins and stabilizes long-range ordering. Also, because of their small energy scales, the magnetic properties of Y_2BaCuO_5 and $BaNi_2V_2O_8$ can be accessed rather easily and their study may yield significant

clues for understanding the magnetic properties of the high-T_C cuprates.

In the future, single crystals of Y_2BaCuO_5 should be studied to determine the nature of the anisotropy and of the magnetic exchange (e.g. from susceptibility and neutron scattering measurements). Pulsed magnetic fields could also be used to extend the phase diagram of Y_2BaCuO_5 to higher fields. Finally, it would be interesting to try to decrease by doping the strength of the exchange interactions, in order to enter into a paramagnetic conducting phase and to study the properties of the related metal–insulator crossover.

Acknowledgments

We would like to thank K-P Bohnen and R Heid for providing us the *ab initio* calculations of the phonon contribution to the specific heat of $YBa_2Cu_3O_7$. This work was supported by the Helmholtz-Gemeinschaft through the Virtual Institute of Research on Quantum Phase Transitions and project VH-NG-016.

References

[1] Jurgens M J, Burlet P, Vettier C, Regnault L P, Henry J Y, Rossat-Mignod J, Noel H, Potel M, Gougeon P and Levet J C 1989 *Physica* B **156/157** 846
[2] Nakano T, Oda M, Manabe C, Momono M, Miura Y and Ido M 1994 *Phys. Rev.* B **49** 16000
[3] Thalmeier P, Zwicknagl G, Stockert O, Sparn G and Steglich F 2005 *Frontiers in Superconducting Materials* (Berlin: Springer) chapter 3
[4] Flouquet J, Knebel G, Braithwaite D, Aoki D, Brison J P, Hardy F, Huxley A, Raymond S, Salce B and Sheikin I 2006 *C. R. Physique* **7** 22
[5] Storey J G, Tallon J L and Williams G V M 2007 *Phys. Rev.* B **76** 174522
[6] Liang W Y and Loram J W 2004 *Physica* C **404** 230
[7] Ong E W, Ramakrishna B L and Iqbal Z 1988 *Solid State Commun.* **66** 171
[8] Goya G F, Mercader R C, Steren L B, Sánchez R D, Causa M T and Tovar M 1996 *J. Phys.: Condens. Matter* **8** 4529
[9] Meyer C, Hartmann-Boutron F, Gros Y, Strobel P, Tholence J L and Pernet M 1990 *Solid State Commun.* **74** 1339
[10] Gros Y, Hartmann-Boutron F, Odin J, Berton A, Strobel P and Meyer C 1992 *J. Magn. Magn. Mater.* **104–107** 621
[11] Matsuo T, Kohno K, Inaba A, Mochida T, Izuoka A and Sugawara T 1998 *J. Chem. Phys.* **108** 9809
[12] Lashley J C, Hundley M F, Migliori A, Sarrao J L, Pagliuso P G, Darling T W, Jaime M, Cooley J C, Hults W L, Morales L, Thoma D J, Smith J L, Boerio-Goates J, Woodfield B F, Stewart G R, Fisher R A and Phillips N E 2003 *Cryogenics* **43** 369
[13] Bohnen K-P, Heid R and Krauss M 2003 *Europhys. Lett.* **64** 104
[14] Bloembergen P 1977 *Physica* B **85** 51
[15] Knafo W, Meingast C, Grube K, Drobnik S, Popovich P, Schweiss P, Adelmann P, Wolf Th and Löhneysen H v 2007 *Phys. Rev. Lett.* **99** 137206
[16] Vollhardt D 1997 *Phys. Rev. Lett.* **78** 1307
[17] Suh B J, Borsa F, Miller L L, Corti M, Johnston D C and Torgeson D R 1995 *Phys. Rev. Lett.* **75** 2212
[18] Sumarlin I W *et al* 1995 *Phys. Rev.* B **51** 5824
[19] Villain J and Loveluck J M 1977 *J. Physique* **38** L77
[20] De Groot H J M and De Jongh L J 1990 *Magnetic Properties of Layered Transition Metal Compounds* ed L J DeJongh (Dordrecht: Kluwer–Academic) pp 379–404
[21] Baum L A, Goeta A E, Mercader R C and Thompson A L 2004 *Solid State Commun.* **130** 387
[22] Ohta H, Kimura S and Motokawa M 1995 *J. Phys. Soc. Japan* **64** 3934
[23] Chattopadhyay T, Brown P J, Köbler U and Wilhelm M 1989 *Europhys. Lett.* **8** 685
[24] Golosovsky I V, Böni P and Fischer P 1993 *Solid State Commun.* **87** 1035
[25] Knafo W, Meingast C, Grube K, Drobnik S, Popovich P, Schweiss P, Adelmann P, Wolf Th and Löhneysen H v 2007 *J. Magn. Magn. Mater.* **310** 1248
[26] De Jongh L J 1990 *Magnetic Properties of Layered Transition Metal Compounds* ed L J DeJongh (Dordrecht: Kluwer–Academic) pp 1–47
Berezinskii V L 1971 *Sov. Phys.—JETP* **32** 493
Kosterlitz J M and Thouless D J 1973 *J. Phys. C: Solid State Phys.* **6** 1181
[27] Rogado N, Huang Q, Lynn J W, Ramirez A P, Huse D and Cava R J 2002 *Phys. Rev.* B **65** 144443
[28] Johnston D C, Sinha S K, Jacobson A J and Newsam J M 1988 *Physica* **153–155** 572
[29] Cuccoli A, Roscilde T, Tognetti V, Vaia R and Verrucchi P 2003 *Phys. Rev.* B **67** 104414